Langmuir
Article
pubs.acs.org/Langmuir

Self-Assembly and Ripening of Polymeric Silver−Alkanethiolate Crystals on Inert Surfaces

Liang Hu, Zishu Zhang, Ming Zhang, Mikhail Y. Efremov, Eric A. Olson, Lito P. de la Rama, Ravi K. Kummamuru, and Leslie H. Allen*

Department of Materials Science and Engineering, Coordinated Science Laboratory, University of Illinois at Urbana−Champaign, Urbana, Illinois 61801

Received March 13, 2009. Revised Manuscript Received May 15, 2009

We characterize and compare the reaction of alkanethiol with Ag continuous planar thin films and Ag islands on inert substrates. Ag islands generate a significantly larger (3-fold) amount of alkanethiolate than continuous Ag films at comparable conditions. The reaction with planar Ag thin films produces alkanethiol self-assembled monolayers (SAMs), whereas the reaction with Ag islands yields two dissimilar products depending on the size of the islands. Small Ag islands are more likely to be converted into multilayer silver−alkanethiolate (AgSR) crystals, while larger Ag islands form monolayer-protected clusters (MPCs). The AgSR lamellar crystals are initially small having only a few layers. However, during thermal annealing, ripening occurs that generates large AgSR lamellae having diameters of 1 μm and thickness up to 30 layers. Atomic force microscopy shows the single-layer step-heights of individual crystals which match the layer thickness obtained via X-ray diffraction analysis. The crystals have facets and flat terraces with extended area, and have a strong preferred orientation (010) normal to the substrate surface. The MPCs move laterally upon annealing and reorganize into a single-layer network with their separation distance approximately equal to the length of an extended alkyl chain.

I. Introduction

Metal−thiolate complexes (metal = Au, Ag, Cu, etc.) are currently of growing technological and scientific interest. The transition of metal−alkanethiolate to nanoparticles upon electron beam irradiation makes it a potential material for electron beam writing.[1,2] Recent studies also demonstrated the luminescent properties of metal−thiolate complexes.[3,4] Luminescence of metal complexes has long been a research interest for applications in photoactive reagent,[5] light-emitting diode,[6] and sensors for volatile organic compounds.[7] Metal−thiolate complexes are also important in the liquid-phase synthesis of metallic nanoparticles as it is considered to be an intermediate product in the reaction sequence.[8,9] Metal−thiolate complexes, monolayer-protected clusters (MPCs), and self-assembled monolayers (SAMs) on extended metal surfaces are the three major species in the binary system composed of metal and thiolate.[10] One of the key differences among them is the S/metal ratio. Among the metal−thiolate complexes, the polycrystalline polymeric silver−alkanethiolate (AgSR, R = C_nH_{2n+1}) prepared in liquid-phase synthesis has been characterized.[11−18] Our research is focused on the synthesis and characterization of AgSR single crystals on inert surfaces.

AgSR has a planar polymeric structure with a −Ag-S− network as the central plane (backbone). Fully extended alkyl chains are bonded to S extending on both sides and are perpendicular to the central plane.[11−18] The arrangement of the alkyl chains in AgSR is analogous to that in 2-dimensional (2D) SAMs on planar substrate. However, the overall composition ratio of S/Ag and the synthesis method are much different for these two kinds of alkanethiolates. AgSR has the ratio of S/Ag = 1.0 and can be produced by using Ag salts and alkanethiol.[11,12,14] In contrast, 2D SAMs are obtained by immersing a bulk solid (planar Ag substrate) into an alkanethiol solution,[19,20] and the effective overall composition approaches zero (S/Ag → 0) since only the Ag surface reacts with alkanethiol to form alkanethiolate. This reaction is self-limiting, whereby the SAMs once formed act as a

*To whom correspondence should be addressed. E-mail: l-allen9@illinois.edu. Phone: (217) 333-7918. Fax: (217) 333-2736.

(1) Corbierre, M. K.; Beerens, J.; Lennox, R. B. *Chem. Mater.* **2005**, *17*, 5774–5779.
(2) Kim, J. U.; Cha, S. H.; Shin, K.; Jho, J. Y.; Lee, J. C. *J. Am. Chem. Soc.* **2005**, *127*, 9962–9963.
(3) Bachman, R. E.; Bodolosky-Bettis, S. A.; Glennon, S. C.; Sirchio, S. A. *J. Am. Chem. Soc.* **2000**, *122*, 7146–7147.
(4) Cha, S. H.; Kim, J. U.; Kim, K. H.; Lee, J. C. *Chem. Mater.* **2007**, *19*, 6297–6303.
(5) Yam, V. W. W.; Lo, K. K. W. *Chem. Soc. Rev.* **1999**, *28*, 323–334.
(6) Ma, Y. G.; Che, C. M.; Chao, H. Y.; Zhou, X. M.; Chan, W. H.; Shen, J. C. *Adv. Mater.* **1999**, *11*, 852–857.
(7) Fernandez, E. J.; Lopez-de-Luzuriaga, J. M.; Monge, M.; Olmos, M. E.; Perez, J.; Laguna, A.; Mohamed, A. A.; Fackler, J. P. *J. Am. Chem. Soc.* **2003**, *125*, 2022–2023.
(8) Yee, C. K.; Jordan, R.; Ulman, A.; White, H.; King, A.; Rafailovich, M.; Sokolov, J. *Langmuir* **1999**, *15*, 3486–3491.
(9) Chen, S. W.; Templeton, A. C.; Murray, R. W. *Langmuir* **2000**, *16*, 3543–3548.
(10) Negishi, Y.; Nobusada, K.; Tsukuda, T. *J. Am. Chem. Soc.* **2005**, *127*, 5261–5270.
(11) Dance, I. G.; Fisher, K. J.; Banda, R. M. H.; Scudder, M. L. *Inorg. Chem.* **1991**, *30*, 183–187.
(12) Baena, M. J.; Espinet, P.; Lequerica, M. C.; Levelut, A. M. *J. Am. Chem. Soc.* **1992**, *114*, 4182–4185.
(13) Fijolek, H. G.; Grohal, J. R.; Sample, J. L.; Natan, M. J. *Inorg. Chem.* **1997**, *36*, 622–628.
(14) Bensebaa, F.; Ellis, T. H.; Kruus, E.; Voicu, R.; Zhou, Y. *Langmuir* **1998**, *14*, 6579–6587.
(15) Voicu, R.; Badia, A.; Morin, F.; Lennox, R. B.; Ellis, T. H. *Chem. Mater.* **2000**, *12*, 2646–2652.
(16) Voicu, R.; Badia, A.; Morin, F.; Lennox, R. B.; Ellis, T. H. *Chem. Mater.* **2001**, *13*, 2266–2271.
(17) Parikh, A. N.; Gillmor, S. D.; Beers, J. D.; Beardmore, K. M.; Cutts, R. W.; Swanson, B. I. *J. Phys. Chem. B* **1999**, *103*, 2850–2861.
(18) Bardeau, J. F.; Parikh, A. N.; Beers, J. D.; Swanson, B. I. *J. Phys. Chem. B* **2000**, *104*, 627–635.
(19) Laibinis, P. E.; Whitesides, G. M.; Allara, D. L.; Tao, Y. T.; Parikh, A. N.; Nuzzo, R. G. *J. Am. Chem. Soc.* **1991**, *113*, 7152–7167.
(20) Walczak, M. M.; Chung, C. K.; Stole, S. M.; Widrig, C. A.; Porter, M. D. *J. Am. Chem. Soc.* **1991**, *113*, 2370–2378.

protective diffusion barrier preventing further reaction of alkanethiol with the underlying Ag. However, there are exceptions to the protective effect of SAMs. Surface pitting occurs on planar Ag substrates during the reaction with alkanethiol and there is transport of Ag from the surface to the solution.[21] An unexpected large thickness of the adsorbed layer is also detected on planar Ag substrates after a long immersion in alkanethiol solution.[22,23]

This self-protection effect is even weaker for 3-dimensional (3D) SAMs on Ag clusters, i.e., MPCs. MPCs have intermediate composition ratio of $0 < S/Ag < 1$ and can be obtained via the liquid-phase method[24] or aerosol processing approach.[25] The size distribution and S/Ag ratio of MPCs can be systematically varied. For example, MPCs with various sizes and S/Ag ratios can be changed to a nearly monodispersed distribution when refluxed in the presence of excess alkanethiol.[26] The degree of surface curvature associated with the size of MPCs plays an important role in the reaction mechanisms and alters the degree of self-limiting properties of SAMs during the reaction. As the size of the MPCs diminishes, the composition of MPCs approaches that of AgSR. Below some critical diameter, every Ag atom of the MPCs is bonded to an alkyl chain with $S/Ag = 1.0$, and AgSR is expected to be the thermodynamically stable phase.

In this report we introduce a new synthesis method in which both AgSR and MPCs coexist as reaction products. The new method employs the reaction of alkanethiol with nanometer-sized Ag islands on inert substrates: low-residual-stress silicon nitride (SiN_x) and holey-carbon films. This method is similar to the preparation of 2D SAMs on planar substrate, except that the exposed Ag islands have highly curved surfaces. The effect of the curvature weakens the self-limiting effect allowing for the formation and coexistence of both MPCs and AgSR. The advantage of this method is that the size of the islands can be systematically changed and measured before immersion. The disadvantage of this method is that the amount of material is extremely small (nanogram), which requires special characterization techniques such as nanocalorimetry. Nanocalorimetry is especially useful for this study since it is designed for thin-film samples (Figure 1a).[27−30] An example of the reaction products of this new method is included in Figure 1, parts b and c, which show atomic force microscopy (AFM) and scanning electron microscopy (SEM) micrographs of the AgSR crystals. Ag islands react much more aggressively with alkanethiol solution than does a planar Ag substrate, which results in a 3-fold increase on the amount of alkanethiolate assembled on the surface.

The outline of the results section is in the following sequence: First, we show the characterization of 2D SAMs on planar Ag layers. Then we describe the results of the overall reaction of the Ag islands with regard to the amount and morphology of the reaction products, and propose a schematic diagram of the reaction sequence. Finally, a detailed characterization of the AgSR phase is presented. A variety of characterization techniques are employed, some of which are typically reserved for surface science studies. Quantity and composition analysis is accomplished by using Rutherford backscattering spectroscopy (RBS), quartz crystal monitor (QCM), and energy dispersive X-ray spectroscopy (EDS). Particle size distributions are tracked with transmission electron microscopy (TEM). The layer spacing of AgSR is obtained with AFM and X-ray diffraction (XRD). The conformation of alkyl chains is measured by using Fourier transform infrared spectroscopy (FTIR).

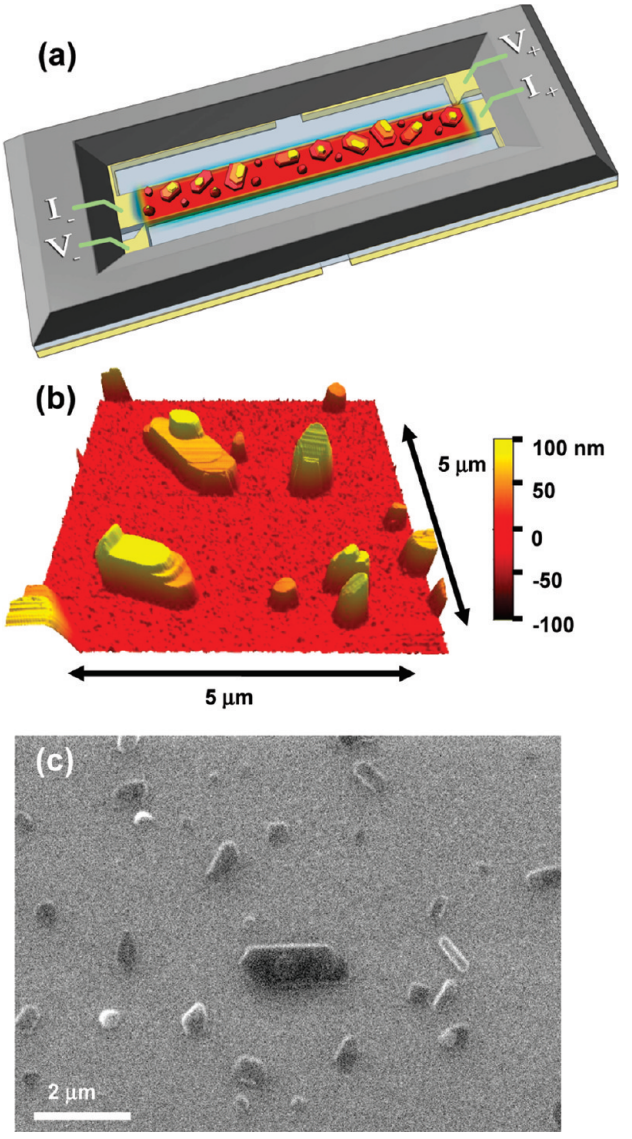

Figure 1. (a) Schematic illustrating the calorimetric measurement of AgSR crystal with nanocalorimetry device. (b) AFM micrograph ($5\,\mu m \times 5\,\mu m$) of AgSC12 crystals grown on SiN_x substrate. (c) SEM micrograph of annealed (120 °C) AgSC12 crystals on SiN_x substrate.

II. Materials and Methods

1. Materials. Silver pellets (99.99%, Kurt J. Lesker Co.) and chrome-plated tungsten rods (R. D. Mathis Co.) were used as vapor deposition sources for Ag and Cr, respectively. 1-Dodecanethiol (≥98%), 1-Tetradecanethiol (≥98%), and 1-Hexadecanethiol

(21) Dhirani, A.; Hines, M. A.; Fisher, A. J.; Ismail, O.; Guyotsionnest, P. *Langmuir* **1995**, *11*, 2609–2614.
(22) Laibinis, P. E.; Whitesides, G. M.; Allara, D. L.; Tao, Y. T.; Parikh, A. N.; Nuzzo, R. G. *J. Am. Chem. Soc.* **1991**, *113*, 7152–7167.
(23) Love, J. C.; Estroff, L. A.; Kriebel, J. K.; Nuzzo, R. G.; Whitesides, G. M. *Chem. Rev.* **2005**, *105*, 1103–1170.
(24) Heath, J. R.; Knobler, C. M.; Leff, D. V. *J. Phys. Chem. B* **1997**, *101*, 189–197.
(25) Harfenist, S. A.; Wang, Z. L.; Alvarez, M. M.; Vezmar, I.; Whetten, R. L. *J. Phys. Chem.* **1996**, *100*, 13904–13910.
(26) Smetana, A. B.; Klabunde, K. J.; Sorensen, C. M. *J. Colloid Interface Sci.* **2005**, *284*, 521–526.
(27) Efremov, M. Y.; Schiettekatte, F.; Zhang, M.; Olson, E. A.; Kwan, A. T.; Berry, R. S.; Allen, L. H. *Phys. Rev. Lett.* **2000**, *85*, 3560–3563.
(28) Lai, S. L.; Guo, J. Y.; Petrova, V.; Ramanath, G.; Allen, L. H. *Phys. Rev. Lett.* **1996**, *77*, 99–102.
(29) Zhang, M.; Efremov, M. Y.; Schiettekatte, F.; Olson, E. A.; Kwan, A. T.; Lai, S. L.; Wisleder, T.; Greene, J. E.; Allen, L. H. *Phys. Rev. B* **2000**, *62*, 10548–10557.
(30) Efremov, M. Y.; Olson, E. A.; Zhang, M.; Zhang, Z. S.; Allen, L. H. *Phys. Rev. Lett.* **2003**, *91*, 085703.

(≥95%) were purchased from Sigma-Aldrich Co. and used as received. Pure ethanol was used as the solvent for alkanethiol, and was purged with dry nitrogen gas to remove dissolved oxygen before use.

Double-side polished (100) Si wafers coated with 30−100 nm of low-residual-stress SiN_x were used as substrates for samples studied with AFM, XRD, SEM, and FTIR. However, there is an intrinsic contaminant of Cl (0.5%) in the SiN_x films. Thus, bare (100) Si wafers with native oxide were used for samples studied with RBS to eliminate the interference from Cl.

2. Sample Preparation and Characterization. *Preparation of 3D Sample on Ag Clusters*. (1) About 0.5 nm of Ag was deposited via thermal evaporation onto the substrates at a rate of 0.05 nm/s. The base pressure was 1×10^{-7} Torr and the pressure during deposition was 5×10^{-7} Torr. A quartz crystal monitor is used during deposition to measure the amount of Ag that was deposited. Cr was not used in the preparation of 3D sample. (2) The samples were then moved out of the vacuum chamber quickly (< 20 min) and immersed into a 1 mM alkanethiol ethanol solution for 48−96 h at room temperature. The solution was sealed from air during the reaction. After the reaction was complete, the samples were then thoroughly rinsed in pure ethanol. (3) The samples were annealed to 120 °C in vacuum (10^{-7} Torr), using a sawtooth heating schedule with an approximate heating rate <25 deg/h and a cooling rate <15 deg/h. The temperature uncertainty is ±2 °C.

Preparation of 2D SAMs on Planar Ag Substrate. (1) The 2D Ag sample had a film stack of Cr (3 nm) and Ag (70 nm). Cr and Ag were vapor deposited at rates of 0.15 and 0.55 nm/s, respectively. The base pressure was 1×10^{-7} Torr, and the pressures during deposition were 5×10^{-6} Torr for Cr and 2×10^{-6} Torr for Ag. The Cr layer provides adhesion between the SiN_x substrate and the Ag layer, and is buried and not exposed to the alkanethiol solution. (2) The reaction process with alkanethiol is the same as step 2 in the preparation of 3D sample on Ag clusters.

Nanocalorimetry. Calorimetric measurements were performed on nanocalorimetry sensors, which were reported in detail elsewhere.[31,32] In brief, a 50-nm-thick Al strip is patterned on a low-residual-stress SiN_x membrane, and works as a heater and a thermometer. Sample was prepared on the other side of SiN_x. A shadow mask made of Si wafer is used for precise alignment of the sample with the Al strip.[33] The misalignment is less than 10 μm. The area of the strip was 2.85 mm^2. The experiments were all performed in vacuum ($< 1 \times 10^{-7}$ Torr). Short current pulses (3−12 ms) were applied through the Al strip, with a 2 s interval for cooling. The heating rate was about 50 000 deg/s. The high sensitivity (< 0.1 nJ/K) and fast scanning rate (15−200 deg/ms) allow us to quantitatively measure the small amount of sample on the surface and characterize the phase transition.[31,32] To obtain the amount of alkanethiolate using nanocalorimetry, we measure the change in the baseline of the heat capacity $\Delta C_p(T)$ ($T = 150$−180 °C) and assume the bulk value of the specific heat of alkane. The uncertainty is about ±2 pmol.

Rutherford Backscattering Spectroscopy. RBS was conducted by using 2 MeV He^+ with 10 nA current, $0.5-2.0 \times 10^{15}$ ions/cm^2 dose, and a beam spot of 3 mm diameter. The effective sample area is about 66 mm^2 considering that the wafer is rotating during the measurement to reduce the effect of ion bombardment on the sample. The amount of Ag and S in the samples was obtained by fitting the experimental spectra to simulations.[34]

Transmission Electron Microscopy. Both SiN_x membranes (≈50 nm thick) and holey carbon Cu grids were used as substrates for TEM study. In contrast to preparing the samples in solution then drop-casting onto membrane, Ag is directly deposited onto the surface of the membrane followed by the reaction with alkanethiol and annealing in vacuum, i.e., all the processes are carried out on the surface. A JEOL 2010 TEM was used at 200 kV to observe the samples on the membrane. Scanning transmission electron microscopy (STEM) mode was used to increase the contrast of imaging. EDS was conducted for local composition analysis.

Atomic Force Microscopy. An Asylum MFP-3D atomic force microscope was used in tapping mode. As shown in Figure 1b, AgSR layer structures with steps were observed on the samples that have reacted with alkanethiol solutions followed by thermal annealing. However, the step height measured in the line scan is accurate only if the layer is not bent and the step edge is parallel to the substrate. Therefore after scanning the sample, we check the 3D topography to choose the line scans that meet this condition to calculate the layer thickness. The tip radius of AFM probes was less than 10 nm. The half-cone angle of the tip was 20−25° along cantilever axis and 10° at the tip apex. The tip convolution is negligible in determining the morphology of the AgSR crystals (Figure 1b), since the diameter (lateral size) of the AgSR crystals is in the order of 1 μm and is about 10 times larger than the thickness (vertical size), which is less than 100 nm. In addition, the separation distances among the AgSR crystals are in the order of 1 um, which are much larger than the tip radius. However, the tip convolution with MPCs can affect the size measurement of MPCs, since the diameters of MPCs and the separation distances are smaller than 10 nm. Therefore, an assembly of separated MPCs would be observed as a continuous film with AFM, and the average height of MPCs would be underestimated. This will be specifically addressed in the appropriate section.

X-ray Diffraction. The X-ray diffraction was performed on a Philips X'pert diffractometer that measures data in reflection mode with Cu Kα (1.5418 Å) radiation at 45 kV and 40 mA. Scans were performed with 0.01° angle resolution.

Scanning Electron Microscopy. A JEOL 6060LV SEM was used, with an accelerating voltage of 10 kV. Since long-time exposure of AgSR to the electron beam can destroy the layer structure, SEM micrographs were taken immediately after moving the microscope's viewing area to an unexposed area of the sample.

Infrared Spectroscopy. Infrared spectroscopy was performed in a Thermo Nicolet Nexus 670 FTIR. Double-side polished Si wafers (500 μm thick) with SiN_x coated on both sides were chosen as sample substrates. A freshly deposited Au mirror was placed on top of the wafer, and IR absorbance spectra were taken by the reflection of the incident beam at a fixed angle of 75°. Background spectra were taken on the same blank substrate with the Au mirror on top. A mercury−cadmium−telluride (MCT) detector was used with liquid nitrogen cooling. Spectra were taken at 1 cm^{-1} resolution. The signal-to-noise ratio is improved by averaging over 128 scans.

III. Results

1. Reaction between Planar Ag Film and Alkanthiol—2D SAMs. When a planar polycrystalline layer of Ag reacts with alkanethiol, 2D SAMs form on the surface. We confirmed this result

(31) Efremov, M. Y.; Olson, E. A.; Zhang, M.; Schiettekatte, F.; Zhang, Z. S.; Allen, L. H. *Rev. Sci. Instrum.* **2004**, *75*, 179.
(32) Olson, E. A.; Efremov, M. Y.; Zhang, M.; Zhang, Z. S.; Allen, L. H. *J. Micro-Electro-Mech. Syst.* **2003**, *12*, 355–64.
(33) Kummamuru, R. K.; Hu, L.; Cook, L.; Efremov, M. Y.; Olson, E. A.; Allen, L. H. *J. Micromech. Microeng.* **2008**, *18*, 095027.
(34) Mayer, M. *Proceedings of the15th International Conference on the Application of Accelerators in Research and Industry*, Denton, Texas, 1999.

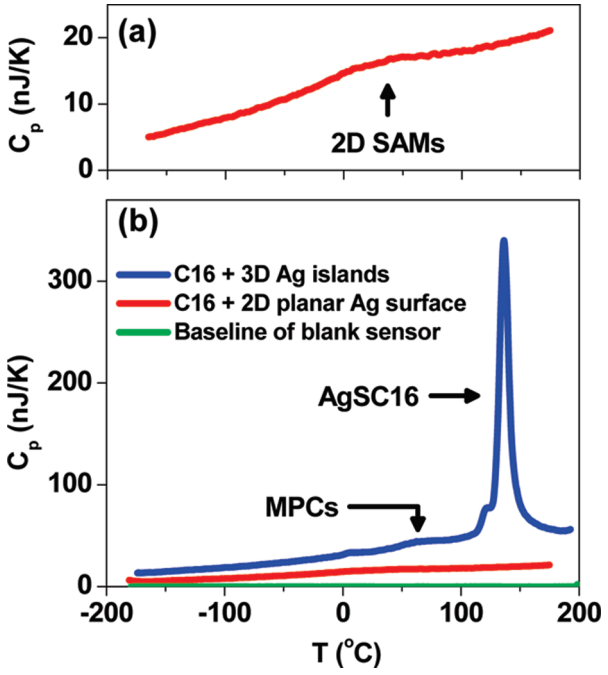

Figure 2. (a) Calorimetric measurement ($C_p(T)$ vs. T) of the 2D hexadecanethiol SAMs on planar Ag substrate. (b) Comparison of $C_p(T)$ of the reaction products of hexadecanethiol with 3D Ag islands (blue curve) and 2D planar Ag substrate (red curve). The green curve is the baseline of the blank nanocalorimetry sensor (within ±0.2 nJ/K).

by depositing 70 nm of Ag on a SiN_x substrate of a nanocalorimetry sensor and then immersing it into an alkanethiol solution.[35] The $C_p(T)$ measurements (Figure 2a) of the reacted film show the same 2D SAMs characteristics as observed in our previous work using planar Au films.[35]

Both Ag and Au samples show the same characteristics of the order−disorder transition, which is very broad and extends over a wide ($\triangle T \approx 50$ °C) temperature range. The peak of this transition is very shallow (the height of the peak $\Delta C_p(T)$ is approximately equal to 2 nJ/K). No sharp phase transitions are evident over the temperature range from −200 to 150 °C (Figure 2a). Both Ag and Au also show about a monolayer of alkanethiol on the surface. The amount of alkanethiolate on the Ag surface is slightly higher (30%) than expected (25 pmol) based on the ideal packing on Ag-(111) (0.185 nm^2/molecule),[36] whereas in the planar Au case there is 30% less than expected (22 pmol) compared to the ideal packing on Au(111) (0.216 nm^2/molecule).[37] In this report we often quote the amounts of material in terms of picomoles by normalizing the value of heat capacity to the fixed area of our nanocalorimetry sensor, which is 2.85 mm^2.

2. Reaction between Ag Islands and Alkanthiol—AgSR and MPCs. In contrast to the planar Ag film, when a discontinuous film consisting of Ag islands, which are made by depositing 0.5 nm of Ag on an inert surface, is immersed into the alkanethiol solution, a large amount of alkanethiol reacts with the Ag. A strong melting transition is observed in the $C_p(T)$ scan as shown in Figure 2b. The height of the melting transition peak is equal to 200−1700 nJ/K in the $C_p(T)$ data as shown in Figure 2b.

(35) Zhang, Z. S.; Wilson, O. M.; Efremov, M. Y.; Olson, E. A.; Braun, P. V.; Senaratne, W.; Ober, C. K.; Zhang, M.; Allen, L. H. *Appl. Phys. Lett.* **2004**, *84*, 5198.

(36) Fenter, P. In *Self-Assembled Monolayers of Thiols*; Ulman, A., Ed.; Academic Press: San Diego, CA, 1998; p 128.

(37) Nuzzo, R. G.; Zegarski, B. R.; Dubois, L. H. *J. Am. Chem. Soc.* **1987**, *109*, 733–740.

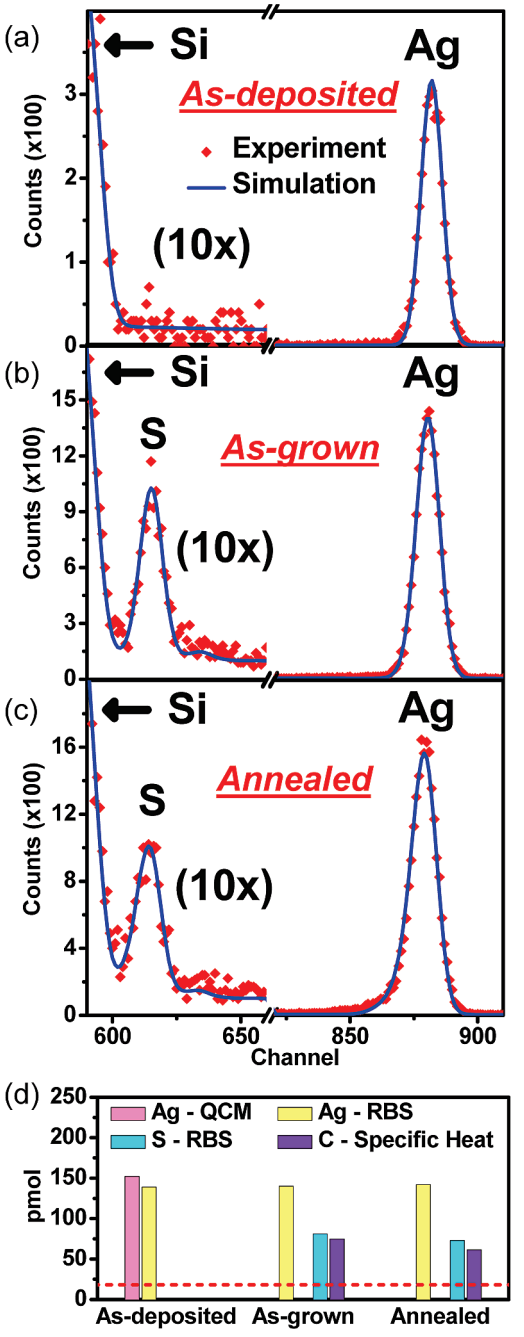

Figure 3. RBS spectra of samples after each process step: (a) Ag deposition (0.51 nm); (b) reaction with hexadecanethiol; and (c) annealed at 120 °C in vacuum. The counts differ from sample to sample because the counting time is different. (d) A summary of the amount of Ag, S, and hexadecanethiolate (C16) characterized by QCM, RBS, and specific heat measurement, respectively. The red dashed line indicates the amount of alkanethioalte based on a model in which all of the Ag islands transform into MPCs.

This value is 10 000% larger than the value we observed in the planar Ag case ($\Delta C_p(T) \approx 2$ nJ/K). Obviously, there is a significant difference in the reaction products between planar Ag films and Ag islands. In the following section we track the molar amounts of Ag, S, and alkanethiolate at each stage of the three process steps: (1) as-deposited (Ag islands), (2) as-grown (small AgSR crystals and MPCs), and (3) annealed (large AgSR crystals and MPC network).

2.1. Composition and Amount of Reaction Products. The average composition (Figure 3) is obtained by using RBS (Ag and S)

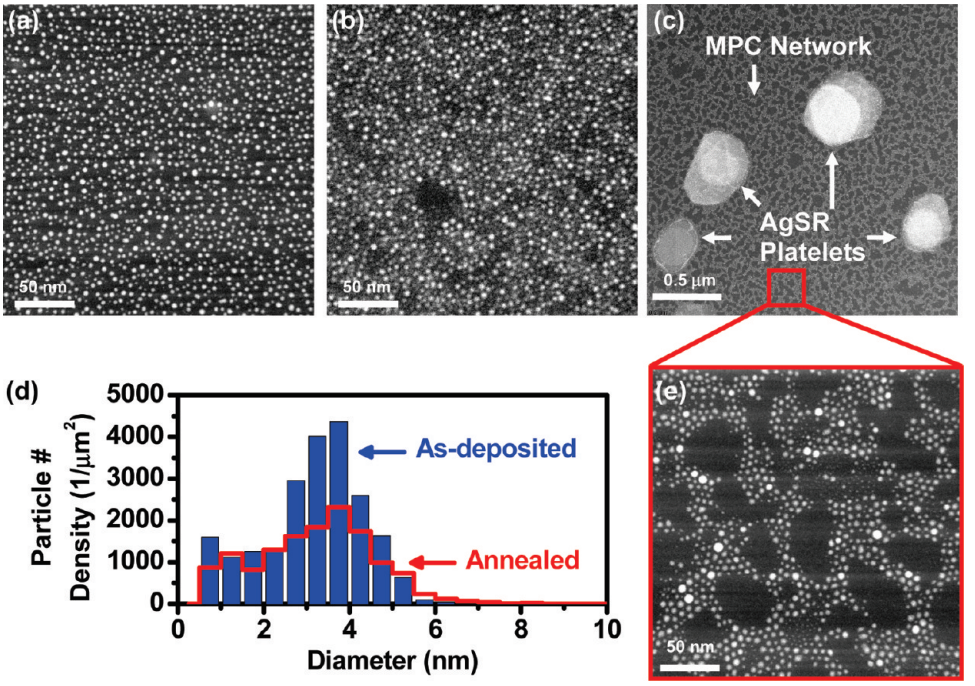

Figure 4. STEM micrographs of the samples after each process step: (a) the as-deposited Ag islands on surface; (b) after the reaction with hexadecanethiol; (c) after annealing at 120 °C in vacuum, two phases form and are separated: the MPC network and AgSC16 crystals. (d) The comparison of particle number density in part a (as-deposited, blue column) and part e (annealed, red step). (e) The magnified micrograph of the MPC network in part c.

and $\Delta C_p(T)$ (alkyl chain) analysis. The results of one particular experiment (hexadecanethiol) are shown in Figure 3 for each step in the process sequence.

The amount of Ag in the as-deposited films is 0.51 nm (140 pmol) as measured with RBS shown in Figure 3a, which is within experimental error equal to the amount measured by using a crystal monitor during the deposition. It is critical to note that the amount of Ag remains constant throughout the processing sequence indicating that only a small amount if any (< 0.01 nm) Ag is lost to the solution during the growth.[38] This result is extremely useful when establishing a model for the reaction process.

The amount of alkanethiolate present on the sample is measured by using the $\Delta C_p(T)$ technique. After immersion the amount of alkanethiolate increases substantially. This increase is 500% more than that expected based on a model where all of the Ag islands transform into MPCs, which would generate only about 15 pmol of alkanethiolate (red dashed line in Figure 3d). During the final step of the process (annealing) the amount of alkanethiolate slightly decreases (≈10%). The bar graph in Figure 3d summarizes these results.

The amount of S is also measured by using the RBS technique. Little if any S is observed in the as-deposited Ag sample. This is important since tarnishing of Ag with the formation of Ag_2S occurs fast for Ag nanoparticles.[39,40] Tarnishing is reduced in our experiments by limiting the total exposure time to the ambient air to less than 20 min. After immersion, the molar amount of S substantially increases and matches (within experimental error) the increase of the molar amount of alkanethiolate (calculated through $\Delta C_p(T)$). During the subsequent annealing step, the amount of S and alkanethiolate both decrease by the same amount, which is a small but measurable (≈10%) quantity. The agreement between the molar amounts of S and alkanethiolate indicates that alkanethiol is the main source of the S in this experiment.

2.2. Morphology during Phase Formation and Separation. TEM micrographs obtained with the STEM mode (Figure 4) show the morphological evolution of the reaction products after each process step.

As-Deposited Sample. Figure 4a shows a discontinuous film was produced consisting of Ag islands with a narrow size distribution. The average diameter is 4.0 nm and the full width at half-maximum (fwhm) is 2.0 nm (based on volume). The density (1.9×10^4 islands/μm^2), average diameter, and spacing of the Ag islands are consistent with the Volmer−Weber growth model for metals deposited on an inert substrate.

As-Grown Sample. After the immersion and the reaction with alkanethiol, the as-grown sample consists of a mixture of two phases—AgSR and MPCs—forming a composite layer in the form of a dense thin continuous sheet.

$$\text{Ag islands} + \text{RSH} \rightarrow \text{AgSR and Ag MPCs}$$

AFM analysis of the samples indicates that the surface of this composite layer is relatively smooth (rms = 1.7 ± 0.2 nm), uniform, and featureless. We deduce that the thickness of the layer of AgSR and MPCs is uniform at least to the level of the substrate roughness (rms = 0.8 ± 0.2 nm). To measure the thickness, a patterned sample was prepared prior to immersion. A contact shadow mask was used during the Ag deposition that generated an array of (7.5 μm × 7.5 μm) Ag squares which are well separated from each other in a checkerboard pattern. During the immersion, the reaction only occurs at the Ag squares (Figure 5a), and provides the contrast for measuring the thickness at the edges of the Ag squares. An AFM line-profile (averaged over 200 line scans) and a height-histogram of as-grown sample are shown in

(38) Edinger, K.; Golzhauser, A.; Demota, K.; Woll, C.; Grunze, M. *Langmuir* **1993**, *9*, 4–8.
(39) McMahon, M.; Lopez, R.; Meyer, H. M.; Feldman, L. C.; Haglund, R. F. *Appl. Phys. B: Lasers Opt.* **2005**, *80*, 915–921.
(40) Graedel, T. E. *J. Electrochem. Soc.* **1992**, *139*, 1963–1970.

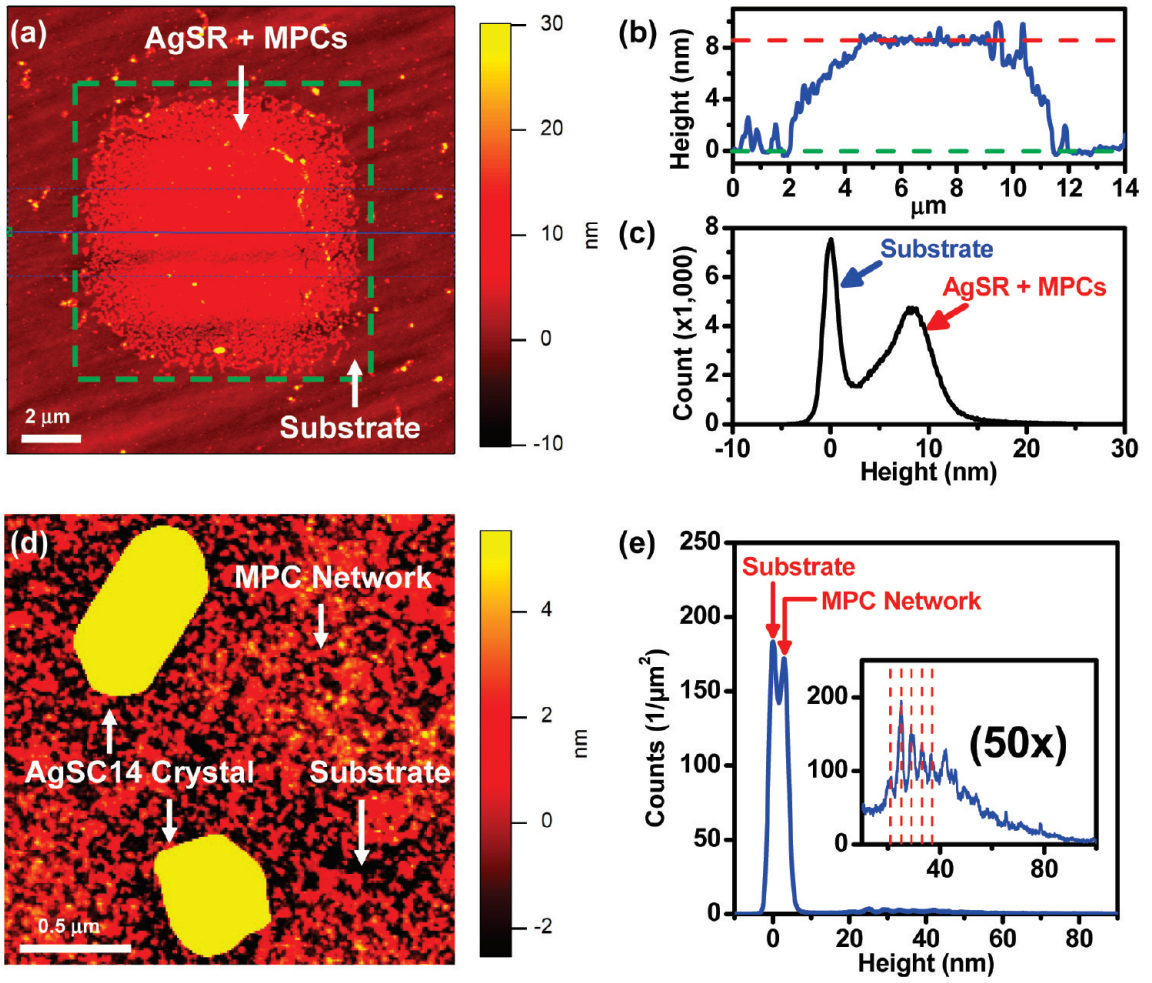

Figure 5. (a) AFM micrograph (15 μm × 15 μm) of a patterned sample. About 0.5 nm of Ag is deposited into a square area of 7.5 μm × 7.5 μm (in the center) and reacts with hexadecanethiol. (b) Average of 200 line scans (area in between the blue dash lines in part a). (c) Histogram of the height data inside the area of the green square in part a. (d) AFM micrograph (2 μm × 2 μm) of the annealed (120 °C) reaction products of deposited Ag islands with tetradecanethiol. Two morphological regions are observed: the MPC network (red) and AgSC14 crystals (yellow). (e) Histogram of the height data over 300 μm^2 area of the sample shown in part d. The inset is a magnification (50×) of the histogram in the height range of 25−90 nm.

Figure 5, parts b and c, respectively, which indicate that the average thickness of the composite sheet of MPCs and AgSR is about 8.6 nm. On the other hand, by using the amount of alkanethiolate obtained with RBS measurement and $\Delta C_p(T)$ analysis, we estimate the thickness of the composite layer to be 8.4 nm, assuming the density equals that of alkanethiol. The agreement between these two values indicates that the composite layer of AgSR and MPCs is a fairly dense (≈90% that of alkanethiol) film.

TEM analysis shows that the as-grown samples are similar to the as-deposited samples. TEM is most sensitive to the location of Ag and not the alkyl chains. At this stage of the reaction sequence, we could not distinguish the AgSR from the MPC phase via TEM images due to the lack of contrast of the thin uniform AgSR crystals. Although it appears that there are more Ag particles in the as-grown sample, we suggest that this is actually an artifact of the e-beam decomposing the AgSR into small Ag particles. Although AgSR is not clearly distinguishable at this stage of the process using AFM or TEM, its presence is easily observed from XRD and calorimetry analysis and will be discussed in the later sections.

Annealed Sample. Upon annealing, the AgSR and MPC phases spatially separate and can be clearly distinguished from each other by using AFM, TEM, SEM, and EDS. AgSR undergoes long-range (1000 nm) transport and ripens into large AgSR platelets (the bright areas in Figure 4c). The MPCs reorganize locally into a single-layer network, which requires only short-range (10 nm) mass transport (Figure 4, parts c and e). The MPCs do not "climb" to form multilayer structure. This is in contrast to the AgSR crystals which form up to 30 layers. The MPC network layer is distributed uniformly on the surface, while the AgSR platelets are localized to only 10% of the surface area. These platelets are easily imaged on all the substrates by using AFM, TEM, and SEM.

TEM micrographs also show that empty patches develop in the annealed samples within the single-layer MPC network region and account for about 35% of the entire sample area. Local composition via EDS analysis confirms that the empty patches are deplete of Ag and S. These patches are generated by two independent processes: (1) the net loss and transport of AgSR out of the region and (2) the movement and spatial reorganization of the MPCs (section IV.2).

The source of the Ag in AgSR is the small Ag islands. In Figure 4d we compare the size distribution of the Ag islands in the as-deposited sample (Figure 4a) with that of the MPCs in the annealed sample (Figure 4e). There is a large reduction (≈30%) in

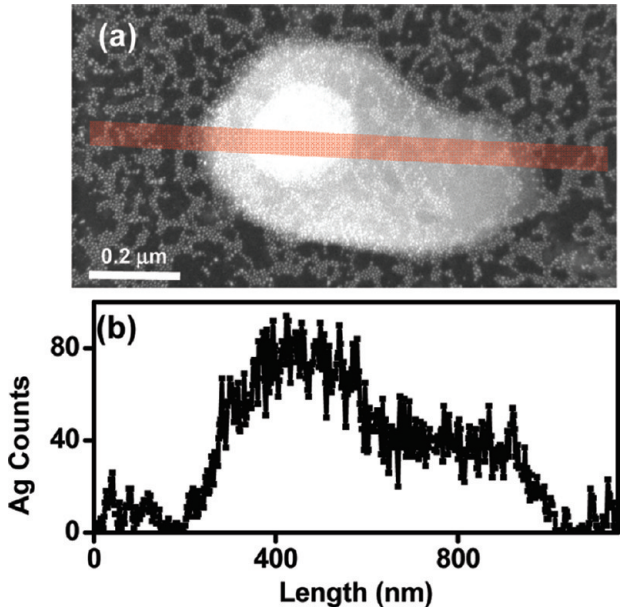

Figure 6. (a) EDS line scan of an AgSC16 crystal along the red line with the length of 1150 nm. The diameter of the beam spot was 0.5 nm. The width of the scanning line is caused by the drift of the sample along the direction perpendicular to the scanning line during the repeated scanning. (b) Average EDS counts of Ag over 30 000 scans on the AgSC16 crystal in part a.

the number of particles (7×10^3 islands/μm^2) especially for particles with diameters less than 5 nm. The missing Ag islands correspond to the Ag in the AgSR phase. The larger Ag islands also react with alkanethiol but survive as MPCs.

AFM micrographs of the annealed samples (Figure 5d) match the TEM micrographs and show the coexistence of two phases. In addition to the lateral spatial arrangement, AFM provides height information of the region. A histogram (Figure 5e) of the height data of a region covering 300 μm^2 area with more than 200 crystals reveals the average properties of many features of the reaction products, including (1) the area (10%) and height of the AgSR crystals, (2) the fine features of the AgSR crystals that indicate texture in the crystal orientation, and (3) the average height (≈3 nm) of the MPCs. The tip convolution of the AFM probe is negligible in analyzing the size of the AgSR platelets, because both the lateral size and separation distance of the AgSR platelets are much larger (≈1 μm) than the tip radius (<10 nm). However, the diameter of the MPCs and the separation distances among them are small (<10 nm). Therefore, the average height of the MPCs is underestimated because of the tip convolution.

We also study the mass transport of AgSR during ripening by tracking the local concentration of Ag using EDS. Figure 6a shows an EDS line scan of Ag in a two-phase region of the same sample as shown in Figure 4c. The result indicates that the average Ag concentration (per unit area) in the AgSR crystals is 6-fold larger than elsewhere (MPC phase plus empty patches). Given the result that Ag is initially uniformly distributed on the surface in the as-deposited sample, we estimate that 35% of all of the Ag is laterally transported and accumulated in the AgSR phase during annealing.

On the basis of the morphological results from TEM and AFM analysis, we generate a sketch (Figure 7) of the evolution of the sample through all three stages of the process. The bundling and interdigitation of the alkyl chains on the MPCs are assumed.[41−43]

3. Identification and Characterization of AgSR. *3.1. Composition.* Both AgSR and MPCs have the same elemental constituents (Ag, S, C, and H). However, they differ markedly in their compositional makeup. We analyze the composition of AgSR via EDS in TEM, and choose the annealed samples where AgSR crystals are spatially separated from MPCs. However, since MPC network is distributed uniformly on the surface, AgSR crystals are overlaying on MPCs in the direction of surface normal, as shown in Figure 6a. Therefore, we conduct EDS analysis in two ways to reduce the influence from MPCs.

In the first method, the STEM mode is used with a small electron beam spot (diameter = 0.5 nm). Care is taken to position the probe on the AgSR crystals in the regions that are above the empty patches of the MPC network. The average composition of the AgSR crystals is measured to be S/Ag = 0.7 ± 0.1. In the second method, we assume the MPC network is uniform on the surface. The TEM mode is used in collecting the EDS signal from the regions that are empty of and filled with AgSR crystals, respectively. The signal of the former is then subtracted form the latter, and the average composition of the AgSR crystals is estimated to be S/Ag = 0.9 ± 0.1.

The S/Ag ratios obtained in both methods are much higher than the S/metal ratio of the reported alkanethiolate MPCs, which varies from 0.1 to 0.48, depending on the size of the MPCs and the surface coverage of the SAMs.[44] On the other hand, this composition value is close to but a little smaller than that of AgSR prepared in liquid-phase synthesis, which has S/Ag = 1.0,[14] and we believe this small difference is caused by the interference from MPCs. Therefore, we suggest that the AgSR phase formed in our samples is more in agreement with the ribbon structure model of Ag−alkanethiolate[14,16] rather than other models (e.g., superlattices of MPCs).[45]

3.2. Layer Structure. AFM. The physical dimension and shape of the AgSR crystals are much different than those of MPCs. Figure 8a shows an AFM micrograph of self-assembled AgSC12 crystals after being annealed to 120 °C. The artifact caused by the convolution between AFM probe tip and the AgSC12 crystals is small compared to the actual size as discussed in the early sections and can be neglected. The AgSC12 crystals have the shape of platelet with a typical thickness/diameter aspect ratio of about 1/10. The AgSR structures have many attributes common to crystalline structures including clearly defined steps, facets, and large-area (≈1 μm^2) terraces with low roughness (<1 nm). Many of the crystals have their surface plane near parallel to the substrate surface indicating strong (010) crystal orientation.

A typical AFM line scan is shown in Figure 8b. The measured step heights are integral multiples of 3.45 ± 0.20 nm. This value is consistent with the layer thickness of 3.48 ± 0.01 nm that is obtained via XRD. Interestingly, individual single steps found in the AgSR crystals are rarely identified in macromolecular systems, although they are routinely observed in other single crystal systems (e.g., Si, GaAs). Similar measurements were also performed on AgSC14 and AgSC16 and are shown in Figure 9b. Clearly the AgSR crystals are constructed via layers of equal

(41) Wang, Z. L.; Harfenist, S. A.; Whetten, R. L.; Bentley, J.; Evans, N. D. *J. Phys. Chem. B* **1998**, *102*, 3068–3072.
(42) Luedtke, W. D.; Landman, U. *J. Phys. Chem.* **1996**, *100*, 13323–13329.
(43) Luedtke, W. D.; Landman, U. *J. Phys. Chem. B* **1998**, *102*, 6566–6572.
(44) Hostetler, M. J.; Wingate, J. E.; Zhong, C. J.; Harris, J. E.; Vachet, R. W.; Clark, M. R.; Londono, J. D.; Green, S. J.; Stokes, J. J.; Wignall, G. D.; Glish, G. L.; Porter, M. D.; Evans, N. D.; Murray, R. W. *Langmuir* **1998**, *14*, 17–30.
(45) Sandhyarani, N.; Resmi, M. R.; Unnikrishnan, R.; Vidyasagar, K.; Ma, S. G.; Antony, M. P.; Selvam, G. P.; Visalakshi, V.; Chandrakumar, N.; Pandian, K.; Tao, Y. T.; Pradeep, T. *Chem. Mater.* **2000**, *12*, 104–113.

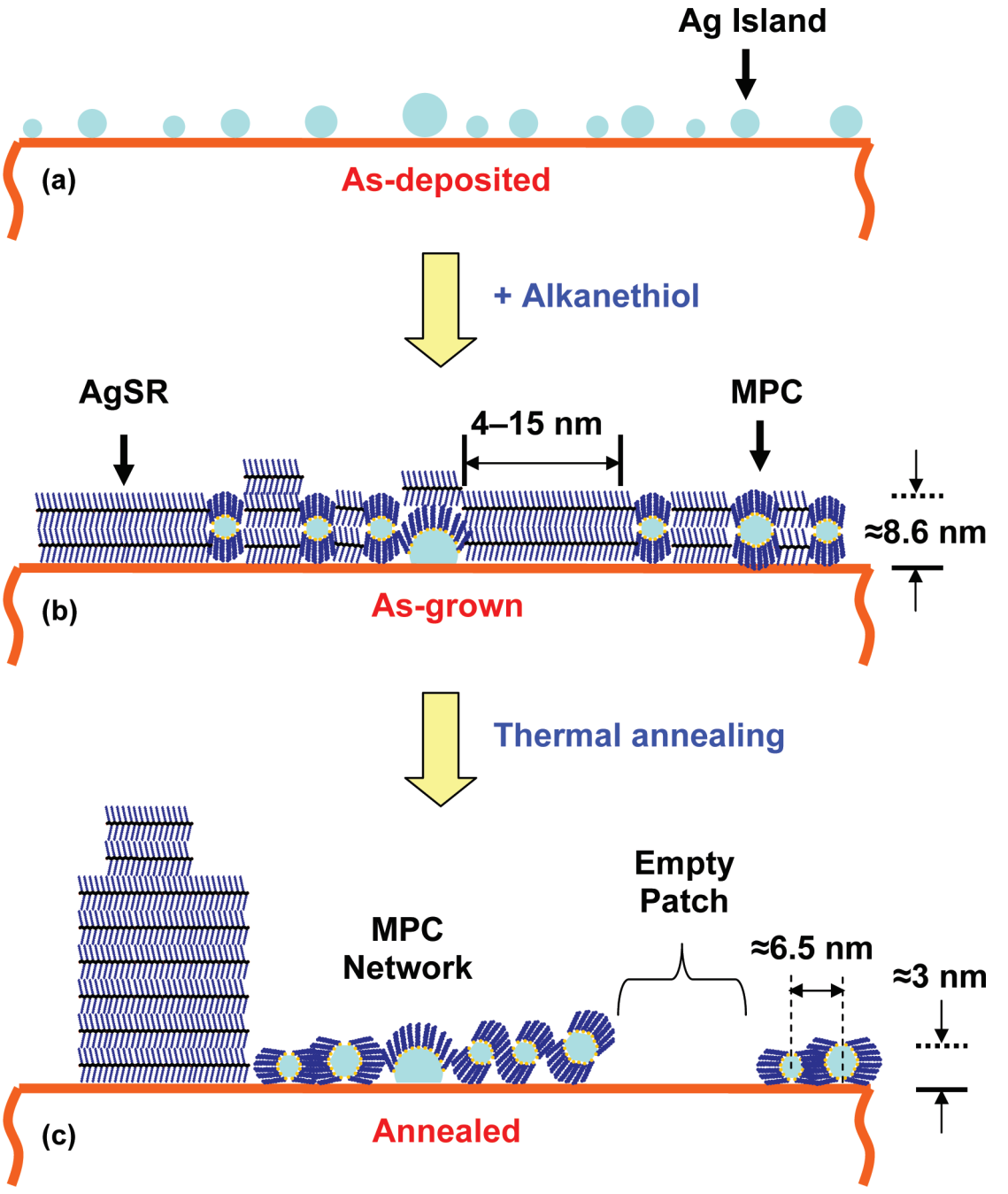

Figure 7. Schematics of the reaction products after each process step: (a) the as-deposited Ag islands on the surface; (b) after the reaction with alkanethiol solution, MPC and AgSR phases form on the entire surface; (c) after annealing at 120 °C in vacuum, the AgSR phase ripens into large crystals, while Ag MPCs reorganize into a single-layer network.

spacing. In addition, the EDS line scan (Figure 6b) also shows large steps in the AgSR crystals.

XRD. Layer structure of AgSR is also observed by using XRD analysis. We note that the XRD diffraction patterns in Figure 9a are only due to the AgSR phase and not the MPC network. Since the diffraction data are collected by using reflection geometry, which provides the information of the sample characteristics in the direction of surface normal, the single-layer MPC network which contains MPCs of various sizes does not give rise to the diffraction pattern. Figure 9a shows the XRD results of self-assembled AgSC12, AgSC14, and AgSC16. The peaks are indexed as a simple multilayer system with (0k0) planes as is done in the studies of AgSR synthesized in solution by others.[14,46] The lattice constant (i.e., the layer thickness) is obtained by least-squares fitting of the strongest 3 or 4 diffraction peaks, but the first peak is not included as it is convoluted with the background signal. The layer thicknesses of the annealed AgSC12, AgSC14, and AgSC16 crystals are 3.48 ± 0.01, 3.95 ± 0.01, and 4.44 ± 0.01 nm, respectively, and are plotted in Figure 9b. Analysis of the dependence of the layer thickness on the chain length is quantified by the length per pair of CH_2 units (dL/dn = 0.242 nm), and the thickness of central −Ag-S− layer plus the terminating CH_3 groups in both ends, which is the intercept (0.817 nm) in Figure 9b. These parameters agree with values reported by others,[14,46] as shown in Table 1.

(46) Levchenko, A. A.; Yee, C. K.; Parikh, A. N.; Navrotsky, A. *Chem. Mater.* **2005**, *17*, 5428–5438.

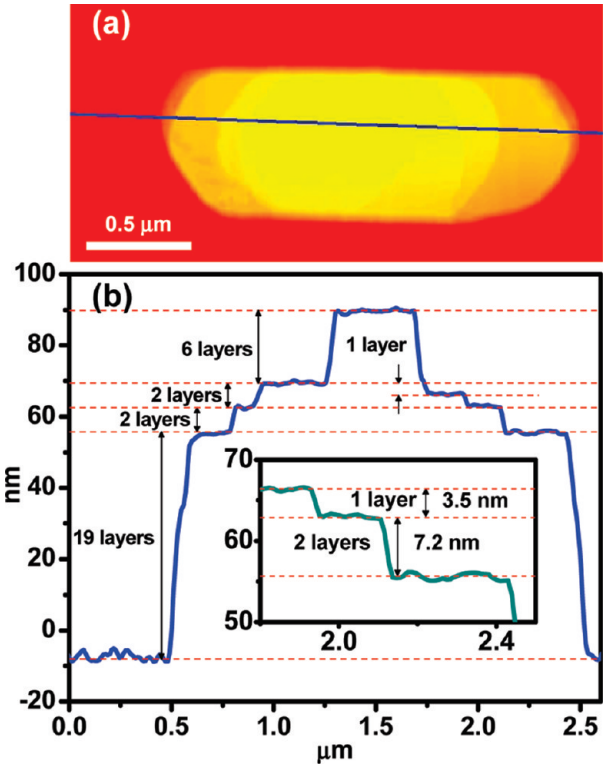

Figure 8. (a) AFM micrograph of an annealed (120 °C) AgSC12 crystal with clearly defined steps, facets, and large-area terraces; (b) the line profile along the blue line in part a.

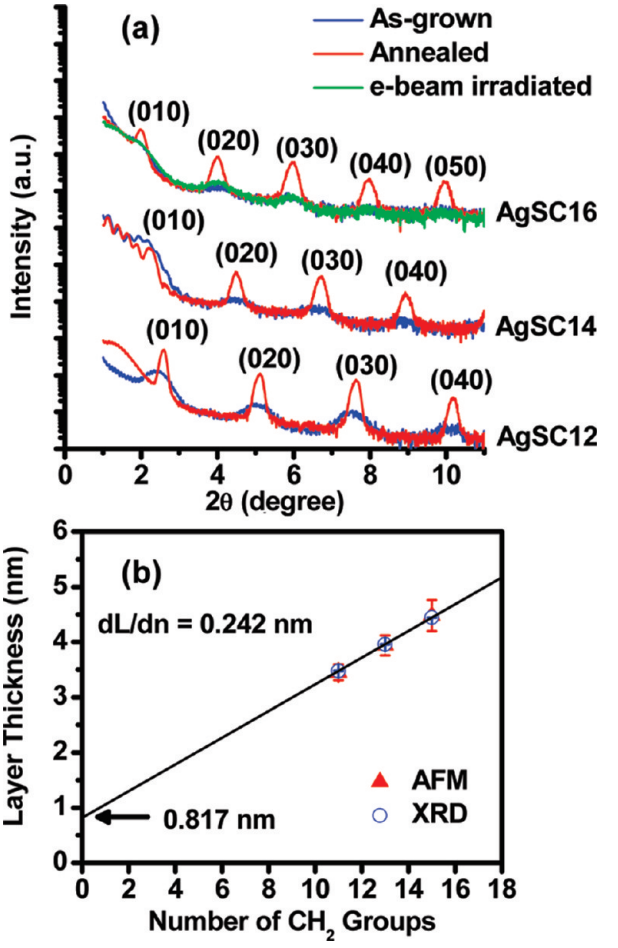

Figure 9. (a) X-ray diffraction patterns of AgSC12, AgSC14, and AgSC16 grown on SiN_x substrate before (blue curve) and after (red curve) annealing. The diffraction peaks are indexed as (0k0). The green curve shows the diffraction pattern of annealed AgSC16 that was irradiated with an electron beam (30 kV, 4 mC/cm^2). (b) Comparison of the layer thickness measured with XRD and AFM. A linear fit of the layer thickness measured via XRD shows the contribution from every pair of CH_2 (dL/dn) is about 0.242 nm, while the thickness of the central −Ag-S− layer plus the terminating CH_3 groups in both ends is about 0.817 nm.

FTIR. Infrared spectroscopy measurements are performed on the as-grown and annealed samples. The peak positions of the symmetric (d+) and antisymmetric (d−) stretching modes of the methylene group (CH_2) are sensitive to the conformational order of the alkyl chains. The d+ and d− modes of AgSC16 peaked at 2847 ± 1.0 and 2915 ± 1.0 cm^{-1}, respectively (Figure 10), which agree with those of AgSC16 bulk samples.[14] Similar results were also obtained on AgSC12 and AgSC14, indicating the self-assembled alkyl chains were fully extended for both the as-grown and annealed samples. Thus, the local interchain structure of AgSR is fairly well established during the growth process. The annealing process only changes the size and shape of the multi-layered structures.

TEM. High-resolution TEM (HRTEM) inspection of the AgSR phase is nebulous because AgSR decomposes due to the effect of the electron beam. Several groups have observed the transition of Au(I)−alkanethiolate to Au nanoparticles upon electron beam irradiation.[1,2] We also observe Ag nanoparticles in the AgSR phase using TEM but we conclude that these are generated by the electron beam itself as we obtain the images. To verify that decomposition occurs in our samples, we expose samples to a 30 kV electron beam with 4 mC/cm^2 dose in a scanning electron microscope. The XRD (green curve in Figure 9a) and IR (green curve in Figure 10) spectra of the sample after exposure clearly show the destruction of the layer structure and conformation due to the electron beam.

3.3. Crystal Size. As-Grown Samples. We did not obtain direct measurements of the thickness or diameter of AgSR in the as-grown samples because we could not image the AgSR crystals using either AFM or TEM at this stage of the process. However, we can estimate the thickness and diameter of AgSR crystals based on our morphology results. For example, for the as-grown sample shown in Figure 5a, if we assume the as-grown AgSC16 lamellae also have (010) preferred orientation (i.e., the lamellae are parallel to the substrate), then we deduce that the average thickness of the as-grown AgSC16 lamellae is equal to or less than the average thickness of the composite layer, i.e., 8.4 nm (<2 layers). To estimate the diameter of the AgSR crystals, we assume that each crystal corresponds to a single Ag island, which is consumed in the reaction with alkanethiol. Then the number of AgSR crystals is approximately equal to the number of missing Ag islands (7×10^3 islands/μm^2).

Table 1. The Length Per Pair of CH_2 Units and the Thickness of the Central −Ag-S− Layer Plus the Terminating CH_3 Groups in Both Ends

	dL/dn (nm)[a]	offset (nm)[b]
This work	0.242	0.817
Bensebaa, et al.[14]	0.246	0.774
Levchenko, et al.[46]	0.241	0.824

[a] dL/dn (slope in Figure 9b) indicates the length per pair of CH_2 units. [b] Offset (the intercept in the axis of layer thickness in Figure 9b) equals the thickness of the central −Ag-S− layer plus the terminating CH_3 groups in both ends.

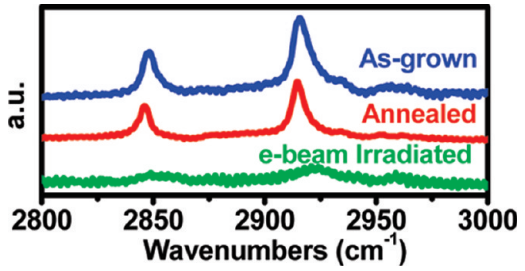

Figure 10. IR spectra of reaction products of 3D Ag islands with hexadecanethiol, illustrating the symmetric (d+) and antisymmetric (d−) stretching modes of the methylene group. The three curves represent different states of the samples: as-grown (blue curve), annealed (120 °C, red curve), and e-beam irradiated (green curve).

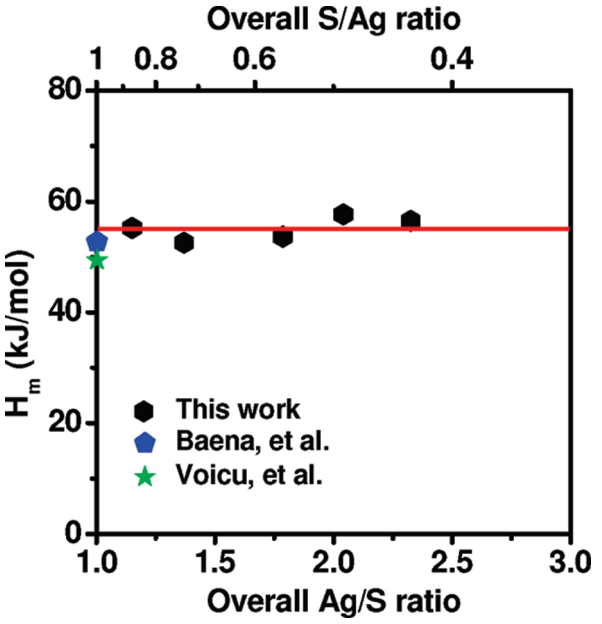

Figure 11. Comparison of molar heat of melting (H_m) of AgSC16 in different experiments. H_m is about 55 ± 5 kJ/mol, independent of the overall Ag/S ratio, and is comparable to the values of the powder AgSC16 samples measured by Baena et al.[12] and Voicu, et al.[15]

The Ag islands with a diameter of 2, 3, 4, or 5 nm will generate 2-layer AgSR crystals with a diameter of 4, 7, 10, or 15 nm, respectively.

Annealed Samples. We do obtain direct measurements of the size of the AgSR crystals for the annealed samples using XRD (thickness), TEM (diameter), and AFM (thickness and diameter). For example, Figure 5e shows the histogram (height vs. frequency) of AFM height data over large areas (300 μm^2, more than 200 crystals). By this means, the average thicknesses for AgSC12, AgSC14, and AgSC16 are measured to be 56 (16.4 layers), 40 (10 layers), and 34 nm (7.7 layers), respectively. Thickness measurements with XRD using Scherrer analysis provides similar values of the thickness.[47] The diameter of the platelets in the annealed samples is large and ranges up to 1 μm. Therefore, annealing the samples increases the average volume of the AgSR crystals by 100-fold due to mass transport driven by the ripening process.

Crystal Texture. The AgSR crystals observed in the annealed samples have a preferred orientation. Texture is evident from the analysis of the AFM height histogram shown in Figure 5e, which includes more than 200 AgSC14 crystals. The peak spacing is about 4.0 nm, consistent with the layer thickness (3.95 nm) of the AgSC14. Furthermore, the relative height (sharpness) of the maxima indicates the crystals have a strong preferred (010) orientation. If a large number of crystals in the sample were randomly oriented, then the histogram would be smooth and featureless. Conversely if the crystals had a high degree of orientation, the histogram would show only a set of discrete lines. For example, in Figure 5e, the sharp peak near the height of 25 nm indicates that about 50% of the crystals of this thickness have (010) texture.

3.4. Melting Transition. Thermal analysis of the thin film samples studied here is not possible with use of conventional DSC instruments since the sample size is too small. Therefore we use the nanocalorimetry technique that is sensitive to sample amount of only nanograms. Another positive attribute is that nanocalorimetry is an absolute measurement technique as is RBS and thus yields molar values for the properties of interest.

The blue curve in Figure 2b shows $C_p(T)$ of the annealed (120 °C) reaction products of hexadecanethiol with Ag islands. A phase transition occurs at $T_m = 137 \pm 3$ °C due to the melting of AgSR. The melting point obtained with nanocalorimetry has a small variation with the heating rate during the measurement. The total amount of self-assembled alkanethiolate (in both AgSR and MPCs) in the sample is calculated via measuring the change in the baseline of the heat capacity $\Delta C_p(T)$. By assuming the composition values of the AgSR phase (S/Ag = 1) and the MPC network phase (S/Ag = 0.12), we calculate the amount of AgSR, whereby the molar heat of melting $H_m = 55 \pm 5$ kJ/mol is obtained. Although the total amount of alkanethiolate and the overall composition S/Ag vary among experiments, the molar value H_m (kJ/mol) of AgSR is independent as shown in Figure 11. The values of T_m and H_m of the transition are comparable (but slightly larger) with the values obtained by Baena et al. and Voicu et al. using conventional DSC on powder AgSR samples which are prepared through liquid-phase synthesis and have overall composition ratio of S/Ag = 1.[12,15] This melting transition is a structural transition from crystal to liquid crystal (mesophases). The layered AgSR crystals undergo a transition to either a lamellar (smectic-A) or a micellar liquid crystal structure.[12]

IV. Discussion

1. Self-Assembly of AgSR. The self-assembly of the layered AgSR phase occurs during the immersion in the alkanethiol solution as indicated by the XRD diffraction peaks and the strong melting transition in the as-grown samples. Since little if any Ag is lost during the reaction, we deduce that the formation of the AgSR phase occurs only at the surface. AgSR does not leave the surface or enter the solution, as it would be highly unlikely that it would return to the substrate. Thus the reaction is localized, which is consistent with the uniform smooth composite layer of AgSR and MPCs.

Due to the curvature of the small islands, the self-assembled monolayers that form on the surface offer less self-protection from further reaction as compared to those on the larger islands and the planar 2D SAMs. In the presence of excess alkanethiol, AgSR forms more easily for small islands since the curvature effect allows more exposure of the Ag surface to the alkanethiol. Additional energy is also gained by maximizing the van der Waals interaction between alkyl chains by changing from a spherical to a layered shape. AgSR can also form directly with adatoms on the substrate surface which diffuse to and from the islands. The adatom flux is greatly enhanced for small clusters.

(47) Cullity, B. D.; Stock, S. R., *Elements of X-ray Diffraction*, 3rd ed.; Prentice Hall: Upper Saddle River, NJ, 2001.

Regardless of the reaction path, each AgSR crystal must nucleate and grow near the island which acts as its source of Ag. We estimate that the number of AgSR nucleation sites will be the same as the number of missing Ag particles as measured from the distribution curves in Figure 4d. Since the islands are initially well separated from each other, much of the AgSR would then form before coalescence occurs. The final result would be a uniform mixture of AgSR and MPCs.

Upon annealing, segments or clusters of AgSR are transported over large distances laterally (≈1000 nm) and vertically (10−100 nm) to form large crystals. On the other hand, the MPCs begin and end as a single layer (vertically) and are limited to a few nanometers in the lateral movement as will be discussed in the next section.

2. Spatial Reorganization of Ag MPCs. In addition to the transport and net loss of Ag from the network region, the spatial arrangement of MPCs also changes during the annealing processes. The MPCs are more ordered compared to the as-deposited Ag islands. For example, we compare the spatial arrangement of the MPCs in the annealed sample (Figure 4e) with that of the Ag islands in the as-deposited sample (Figure 4a). As discussed earlier, the particle density decreases from 1.9×10^4 islands/μm^2 to 1.2×10^4 clusters/μm^2. Assuming the smallest 7×10^4 islands/μm^2 in the as-deposited sample finally transform into AgSR, we only analyze the arrangement of the rest of the large Ag islands in the as-deposited sample which would evolve into MPCs during the reaction. The average center-to-center distance and variance of this distance of the three nearest neighbors decrease from 8.1 ± 1.7 (Ag islands) to 6.5 ± 0.6 nm (MPCs). This change in the spatial reorganization implies that the MPCs move during the growth and the annealing process. As the MPCs move closer to each other, the empty patch areas are generated. This reorganization and movement do not happen for Ag islands at such low temperatures. Spatial ordering has been routinely observed in MPCs which are drop-cast onto a TEM grid,[44] and it is assumed that this type of reorganization occurs as a consequence of the liquid evaporation process.

Although the MPCs move toward one another, there is a lower limit on how close they approach their nearest neighbors. On average, the nearest edge-to-edge separation distance is 2.40 ± 0.45 nm. This separation is consistent with the natural minimum separation due to the self-limiting effect of the extended alkyl chains and their interdigitation, since the fully extended chain length of hexadecanethiol is 2.45 nm.[48] This supports the idea that the growth and the annealing process have transformed many of the large Ag islands into MPCs that are the same as those produced by other methods.[24,25]

V. Conclusion

In summary, we show that the reaction of Ag islands with alkanethiol is much different as compared to planar Ag substrates which generate 2D SAMs on the Ag surface. Ag islands react actively with alkanethiol forming two reaction products: AgSR and MPCs. The small Ag islands are more likely to react to form polymeric AgSR, while the large Ag islands survive and form MPCs, analogous to the monolayer formation on the planar Ag surface.

During the annealing, the AgSR and MPC phases separate. Ripening of the AgSR crystals occurs via long-range (μm) mass transport, which generates large (diameter ≈1 μm) lamellae. XRD and AFM analysis show the AgSR crystals have a layer structure consistent with the AgSR prepared from liquid-phase synthesis. Individual single-layer steps are clearly observed by AFM. The AgSR crystals also show strong (010) texture. Nanocalorimetry analysis shows that the AgSR has similar melting temperature (137 ± 3 °C) and enthalpy (55 ± 5 kJ/mol) as the bulk AgSR. On the other hand, MPCs move closer to each other, reorganizing and forming an ordered network with the separation distance between MPCs approximately equal to the length of fully extended alkyl chains.

Acknowledgment. This work was supported by NSF-DMR-0735286. Fabrication of the shadow mask is supported by NIST-70NANB7H6162 and equipment usage through NSF-ECS-0622117. Microanalysis characterization was carried out in part in the Frederick Seitz Materials Research Laboratory Central Facilities, University of Illinois, which are partially supported by the U.S. Department of Energy under grants DE-FG02-07ER46453 and DE-FG02-07ER46471. The authors thank M. Sardela, S. MacLaren, C. H. Lei, J. G. Wen, D. Jeffers, and J. Soares for their generous help. The nanocalorimetry sensors were fabricated at the Cornell NanoScale Facility, a member of the National Nanotechnology Infrastructure Network, which is supported by the NSF-ECS-0335765.

(48) Porter, M. D.; Bright, T. B.; Allara, D. L.; Chidsey, C. E. D. *J. Am. Chem. Soc.* **1987**, *109*, 3559–3568.